ACS OMEGA

http://pubs.acs.org/journal/acsodf

Article

# Bonding and Tunneling

John F. Wager and Douglas A. Keszler*

Cite This: *ACS Omega* 2023, 8, 23182−23190

Read Online

ACCESS | Metrics & More | Article Recommendations

**ABSTRACT:** Quantum mechanical electron tunneling is proposed as the mediator of chemical bonding. Covalent, ionic, and polar covalent bonds all rely on quantum mechanical tunneling, but the nature of tunneling differs for each bond type. Covalent bonding involves bidirectional tunneling across a symmetric energy barrier. Ionic bonding occurs by unidirectional tunneling from the cation to the anion across an asymmetric energy barrier. Polar covalent bonding is a more complicated type of bidirectional tunneling, consisting of both cation-to-anion and anion-to-cation tunneling across asymmetric energy barriers. Tunneling considerations suggest the possibility of another type of bond—denoted polar ionic—in which tunneling involves two electrons across asymmetric barriers.

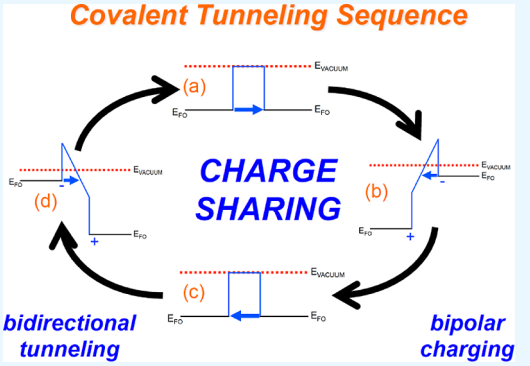


## INTRODUCTION

Chemical bonding presents a deep mystery; it asserts nearest-neighbor coupling and yet depends strongly on long-range Coulombic interactions.[1] How can this be? Understanding the role of tunneling in facilitating chemical bonding is the key to unraveling this puzzle. We assert that chemical bonding is accomplished by quantum mechanical tunneling of electrons. Since the tunneling probability decreases exponentially with distance, chemical bonding interactions involve nearest neighbors almost exclusively. For example, silicon nearest- and second-nearest-neighbor distances are 235 and 384 pm, respectively. Using a tunneling characteristic distance of 45.45 pm for silicon, the nearest-neighbor tunneling probability is 27 times larger than that for second-nearest-neighbor tunneling. Thus, chemical bonding is primarily a nearest-neighbor interaction in most chemical systems because it is mediated by tunneling, whose probability decays exponentially with distance.

Invoking tunneling as a chemical bonding mediator clarifies other chemical conundrums. For example, the bond valence model is extremely useful and is employed by an army of chemists, but it is entirely empirical.[1] Since the bond valence is usually taken to be exponentially dependent upon distance, we assert that electron tunneling is the physical mechanism underlying the bond valence. Another example of tunneling helping to resolve a chemical enigma involves the concept of partial charge. Basic electrostatics dictates that electric field lines begin on the positive charge and terminate on the negative charge. How is it possible to begin or terminate a field line on a partial charge? The concept of partial charge is not a problem if chemical bonding is mediated by electron tunneling since partial charge is simply a time-averaged property of one-at-a-time electron tunneling.

Quantum mechanical tunneling in a chemical system is a topic well discussed in the literature.[2−9] Much of this work is directed to atomic (usually hydrogen) tunneling, rather than electron tunneling. Treatments typically invoke tunneling to clarify subtle issues involving chemical kinetics, chemical dynamics, or chemical reactions. Unfortunately, this literature is not pertinent to the primary themes addressed herein, i.e., identifying quantum mechanical tunneling as the mediator of chemical bonding and elucidating physical principles foundational to the bond valence method.

A distinctive feature of the chemical-bonding-tunneling perspective discussed herein is that it is dynamic. Its dynamic nature can be traced back to the work of Sutton, who deduced the importance of tunneling in chemical bonding by solving the time-*dependent* Schroedinger equation.[10] In contrast, other chemical bonding approaches are invariably static, not dynamic, as they explicitly or implicitly are formulated as a consequence of solving the time-*independent* Schroedinger equation.[11]

The origin of the work presented herein is a series of papers in which we proposed and refined an atomic solid-state energy (SSE) scale.[12−15] This SSE scale is empirical. It was developed

**Received:** April 21, 2023
**Accepted:** May 23, 2023
**Published:** June 12, 2023

as a consequence of our attempts to make sense of two experimentally observed trends:

1. The electron affinity (EA) of a binary solid state compound tends to increase (move toward the vacuum level, $E_{VACUUM}$) with increasing band gap ($E_G$), while the ionization potential (IP) tends to decrease (move away from $E_{VACUUM}$) with increasing band gap.[12,13] This empirical trend in energetic positioning of EA and IP with respect to $E_G$ is found to be symmetric with respect to a universal SSE reference of −4.5 eV with respect to $E_{VACUUM}$, corresponding to the hydrogen donor/acceptor ionization energy, $\varepsilon(\pm)$, or equivalently the standard hydrogen electrode energy.
2. EA and IP of a binary solid state compound tend to increase (move toward $E_{VACUUM}$) and decrease (move away from $E_{VACUUM}$), respectively, with decreasing interatomic distance.[15] This empirical trend in energetic positioning of EA and IP with respect to interatomic distance is also found to be symmetric with respect to $\varepsilon(\pm)$.

Assessment of experimental trend #1 led to the development of the SSE scale, a simple and useful alternative approach to electronegativity and chemical hardness.[12,13] More recently, evaluation of experimental trend #2 clarified the nature of solid-state chemical bonding in terms of charge sharing, charge transfer, and charge redistribution from a static perspective, different from the dynamic approach adopted herein. Also, polar covalent tendency (PCT) was proposed as an improvement to the concept of ionicity, and the Principle of Minimum Charge Transfer was formulated as a simple way to predict the ionic or polar covalent character of a given binary compound family.[15]

The goal of the work presented herein is to clarify the role of quantum mechanical electron tunneling in facilitating the formation of a chemical bond within the SSE conceptual framework. Although we briefly discussed tunneling in a previous publication,[15] only ionic bonding charge transfer via tunneling was considered. In this contribution, we distinguish between bidirectional and unidirectional tunneling and investigate the role of single-electron tunneling in facilitating covalent, ionic, and polar covalent bonding. The key to establishing a link between chemical bonding and quantum mechanical tunneling is formulation of an energy band diagram for each relevant step of the chemical bonding process.

## RESULTS AND DISCUSSION

**Homopolar Bonding.** Figure 1 shows a molecular orbital picture of homopolar or covalent bonding from the perspective of the emergence of antibonding and bonding orbitals. As two identical atoms approach each other from infinity, their frontier orbitals energetically align at $E_{FO}$. Nothing happens in terms of chemical bonding until these atoms are close enough that there is appreciable quantum mechanical overlap of their wave functions. Wave function overlap splits the frontier orbital degeneracy such that antibonding and bonding orbitals emerge above and below $E_{FO}$. As the interatomic distance decreases, the antibonding−bonding energy of separation increases.

A molecular orbital tight-binding model (which ignores the overlap integral to simplify the mathematical complexity of the model[11]) asserts that the energy separating antibonding and bonding orbitals is approximately equal to $2|\beta|$, where $|\beta|$ is the absolute value of the off-diagonal elements of the Hamiltonian

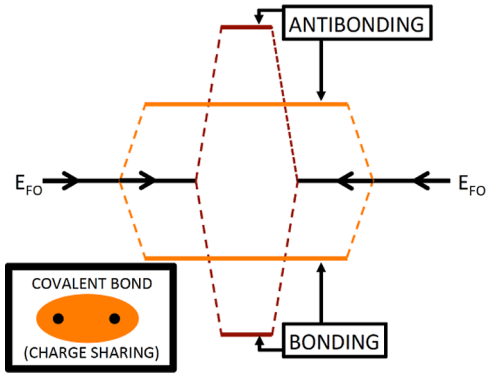


**Figure 1.** Molecular orbital picture of a homopolar (covalent) bond illustrating the formation of antibonding and bonding states due to electronic charge sharing by the frontier orbital (FO) wave function overlap. As the interatomic distance decreases, the antibonding−bonding energy increases.

matrix of the two-atom, homopolar model system.[10] $\beta$ is sometimes referred to as a hopping integral (also sometimes referred to as an exchange, resonance, or bond integral) since the tunneling rate, $R_T$, i.e., the probability per unit time that an electron tunnels (hops) between atoms, is equal to $2|\beta|/h$, where $h$ is Planck's constant. Thus, homopolar (covalent) bonding involves tunneling between constituent atoms; an increase in the tunneling rate leads to an increase in the antibonding−bonding energy via $|\beta|$.

Antibonding and bonding orbitals pertain to atomic or molecular states. In a solid, the antibonding−bonding energy of the separation equivalent is the Penn gap, $E_{PENN}$.[14,16,17] Thus, for an elemental solid, we obtain

$$R_T \approx \frac{2|\beta|}{h} \approx \frac{E_{PENN}}{h} \quad (1)$$

Using eq 1, Table 1 displays estimates of $R_T$ for three elemental solids, diamond (C), silicon (Si), and germanium

**Table 1. Tunneling Rate ($R_T$) and Tunneling Attempt Time ($t_T$) Evaluated for Three Elemental Solids**

| element | Penn gap (eV)[17] | $R_T$ (prob s$^{-1}$) | $t_T$ (fs) |
|---|---|---|---|
| C | 13.5 | $3.3 \times 10^{15}$ | 0.31 |
| Si | 4.77 | $1.2 \times 10^{15}$ | 0.87 |
| Ge | 4.31 | $1.0 \times 10^{15}$ | 0.96 |

(Ge). These tunneling rates are extraordinarily large. To provide a more intuitive feel of just how fast "hopping" occurs, we define a tunneling attempt time, $t_T$, as the reciprocal of $R_T$ multiplied by a probability of 100% and interpret $t_T$ as the reciprocal of a "hopping" attempt frequency. The subfemtosecond (fs) times included in the last column of Table 1 are remarkably fast, as evident from the fact that the equivalent reciprocal thermal attempt frequency ($h/k_BT$) is equal to 160 fs at 298 K, more than two orders of magnitude slower. In summary, these estimates for $R_T$ and $t_T$ reveal that the charge sharing responsible for homopolar (covalent) bonding is mediated by the exchange of electrons via tunneling ("hopping") and that the "hopping" rate is very fast compared to a normal thermal process.

Next, we explore how homopolar (covalent) "hopping" or electron tunneling actually occurs. Figure 2 shows an energy band diagram illustrating covalent bond formation from the


https://doi.org/10.1021/acsomega.3c02736
ACS Omega 2023, 8, 23182−23190

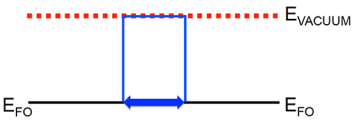


**Figure 2.** Homopolar (covalent) bond formation. Frontier orbitals of identical atoms align energetically such that a symmetric, rectangular tunnel barrier is established. When these atoms are close enough, tunneling occurs in both directions.

perspective of tunneling. As two identical atoms are brought together from infinity, their frontier orbitals have the same energy, $E_{FO}$, which is referenced to the vacuum level, $E_{VACUUM}$. When these atoms are remote from each other, nothing happens in terms of chemical bonding. However, when these atoms get close enough that there is appreciable overlap of their wave functions, tunneling occurs. This tunneling is bidirectional, i.e., electrons tunnel in both directions, from left to right and from right to left. Figure 2 indicates that the tunneling barrier is symmetric and rectangular.

As a brief aside, consider the case of electron tunneling through a symmetric rectangular barrier from a quantitative perspective, as illustrated in Figure 3. The tunneling trans-

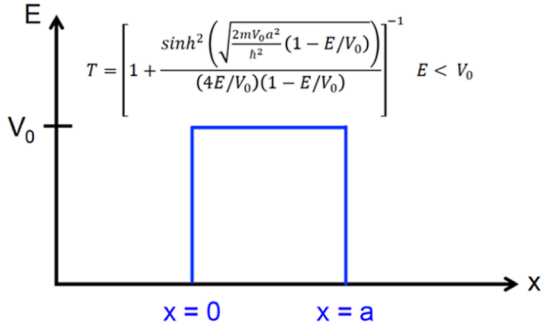


**Figure 3.** Rectangular barrier tunneling. The transmission coefficient ($T$) of an electron with an incident energy ($E$) encountering the left side of a rectangular potential barrier of height $V_0$ and width $a$ is equal to that given by the equation indicated above (as long as $E < V_0$). $m$ = electron rest mass and ħ = reduced Planck constant.

mission coefficient ($T$) strongly depends on the "opacity" of the barrier, i.e., on $2mV_0a^2/\hbar^2$, where m is the electron mass, $V_0$ is the barrier height, $a$ is the barrier width, and ħ is the reduced Planck constant.[18] When the barrier "opacity" is large, the tunneling probability is small; when the barrier "opacity" is small enough, the tunneling probability may become appreciable. Thus, the tunneling tendency (probability) depends on the height and (especially) the width of the barrier, i.e., on $V_0a^2$.

Opacity is a useful concept for understanding tunneling aspects of chemical bonding. To achieve the same tunneling opacity (related to the tunneling transmission probability), a deep frontier orbital requires a shorter interatomic distance than a shallow frontier orbital. This means that the frontier orbital energy determines, to a large extent, the equilibrium interatomic distance of a bond. This strong connection between frontier orbital energy and interatomic distance is a consequence of having bidirectional tunneling through a rectangular barrier as the operative mechanism of covalent bond formation.

Covalent bond formation tunneling dynamics are illustrated in Figure 4. Prior to the onset of tunneling, the two-atom

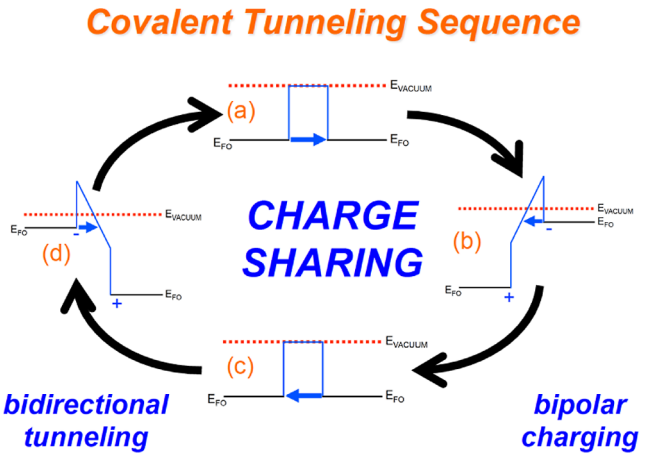


**Figure 4.** Homopolar (covalent) bond formation tunneling sequence. (a) Electron tunnels from the left to right frontier orbital, leading to (b) negative (positive) charging of the right (left) frontier orbital. Next, an electron tunnels from the right to left frontier orbital, (c) neutralizing the charging such that the bond is again charge neutral. Then, an electron tunnels from the right to left frontier orbital, (d) positively (negatively) charging the right (left) frontier orbital. Finally, an electron tunnels from the left to right frontier orbital, neutralizing the charging such that the bond is again charge neutral. This figure illustrates bonding in silicon in which it is assumed that $E_{FO} \approx -4.5$ eV and $U_{\Delta q=1e^-} \approx 6.1$ eV.

system is electrically neutral and the tunneling barrier is symmetric and rectangular, as sketched in Figure 4a. Suppose an electron tunnels from the left to the right frontier orbital, as indicated by the right-going blue arrow in Figure 4a. The tunneling electron negatively charges the right frontier orbital, leaving behind a positively charged left frontier orbital, as shown in Figure 4b. Negative charging pushes the right frontier orbital upward in energy, toward the vacuum level, while positive charging moves the left frontier orbital downward, away from the vacuum level. Charge separation sets up an electric field, as shown by the positive sloping line shown in Figure 4b.

The energy separating the charged frontier orbitals of Figure 4b can be estimated as Coulombic energy as given by (assuming a point charge model)[19]

$$U = \frac{1}{4\pi\varepsilon_0}\frac{(\Delta q)^2}{d} \tag{2}$$

where $\varepsilon_0$ is the dielectric constant of free space, $\Delta q$ is the transferred charge, and $d$ is the interatomic distance. Since one electron is transferred in the process shown in Figure 4, $\Delta q = 1$ such that

$$U_{\Delta q=1e^-} = \frac{1}{4\pi\varepsilon_0 d} = \frac{1439.42}{d\ (\text{pm})}\ \text{eV} \tag{3}$$

where the interatomic distance is expressed in units of picometers (pm). Figure 4 illustrates the expected case of silicon bonding in which $E_{FO} \approx -4.5$ eV and $U_{\Delta q=1e^-} \approx 6.1$ eV since d ≈ 235 pm. Knowing $U_{\Delta q=1e^-}$, we can calculate the electric field of Figure 4b as $U_{\Delta q=1e^-}/d \approx 260$ MV/cm. This is an extraordinarily large value of electric field.

Returning to our discussion of the homopolar tunneling sequence, electron tunneling from the right to the left frontier orbital (left-going blue arrow in Figure 4b) resets the two-atom system back into an electrically neutral state (Figure 4c). Note


https://doi.org/10.1021/acsomega.3c02736
ACS Omega 2023, 8, 23182−23190

that Figure 4b tunneling occurs through a triangular barrier of reduced thickness compared to $d_{Si}$ = 235 pm; this type of tunneling is termed Fowler-Nordheim.[20] Next, if an electron tunnels from the right to the left frontier orbital (left-going blue arrow in Figure 4c, positive (negative) charging pushes the right (left) frontier orbital downward (upward), as indicated in Figure 4d. Note that Figure 4b,d represent similarly charged states, but with opposite polarities.

Finally, electron (Fowler−Nordheim) tunneling from the left to the right frontier orbital (right-going blue arrow in Figure 4d) provides a reset back to the neutral state (Figure 4a). As specified in Figure 4, covalent bonding involves charge sharing via bidirectional tunneling across a symmetric barrier. Bidirectional tunneling leads to bipolar charging in which frontier orbitals can be positively or negatively charged, as well as neutral.

The dynamic tunneling perspective proposed herein suggests that covalent bonding is Coulombic in nature due to charge separation steps of the homopolar bond formation tunneling cycle, as shown in Figure 4b,d.

**Heteropolar Bonding.** Based on tunneling considerations, we distinguish three types of heteropolar bond, i.e., polar covalent, ionic, and polar ionic. First consider polar covalent bonding, as illustrated in Figure 5, for the specific case of

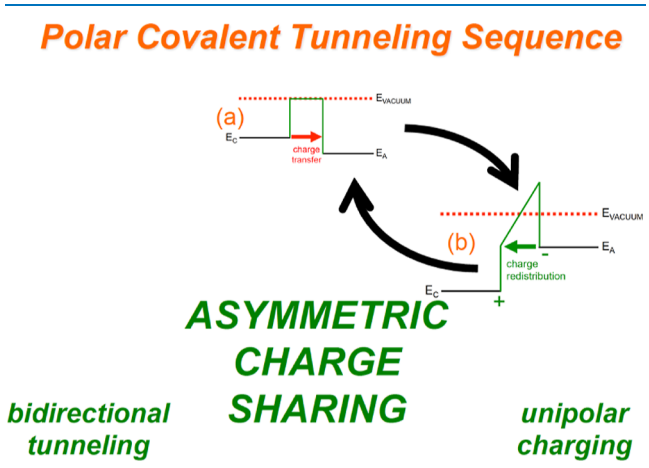


**Figure 5.** Heteropolar (polar covalent) bond formation tunneling sequence. (a) Electron tunnels from the cation to anion frontier orbital (charge transfer), leading to (b) negative (positive) charging of the anion (cation) frontier orbital. Then, an electron tunnels from the charged anion orbital to the charged cation orbital (charge redistribution), neutralizing the charge state such that the bond is again charge neutral. This figure illustrates bonding in gallium arsenide (GaAs) in which it is assumed that $E_C \approx -3.1$ eV, $E_A \approx -5.9$ eV, and $U_{\Delta q=1e^-} \approx 5.9$ eV.

gallium arsenide (GaAs) in which it is assumed that $E_C \approx -3.1$ eV, $E_A \approx -5.9$ eV, and $U_{\Delta q=1e^-} \approx 5.9$ eV since $d \approx 245$ pm. In a heteropolar bond, as the incipient cation and anion are brought closer together from infinity, their frontier orbitals are energetically misaligned, as shown in Figure 5a. The cation frontier orbital, $E_C$, is positioned nearer to the vacuum level than the anion frontier orbital, $E_A$. Thus, there is an energy misalignment driving force favoring electron transfer from the cation to anion in order to lower the overall energy of the two-atom heteropolar system. However, nothing happens in terms of chemical bonding until the cation and anion are close enough that there is an overlap between their wave functions. Once wave function overlap is appreciable, there is a tendency to move electronic charge from the cation to the anion, as shown by the right-going red arrow in Figure 5a. This charge transfer occurs by quantum mechanical tunneling of an electron across an asymmetric rectangular barrier. Electron tunneling leaves the cation positively charged, pushing its frontier orbital downward in energy, away from the vacuum level, while rendering the anion negatively charged, lifting the anion frontier orbital upward in energy, toward the vacuum level, as indicated in Figure 5b. Additionally, a large electric field (240 MV/cm) is set up as a consequence of this charge separation, as evident from the positive sloping portion of the barrier shown in Figure 5b.

After charge transfer, the charged anion frontier orbital is positioned higher in energy than that of the charged cation frontier orbital so that electron tunneling from the anion to the cation (charge redistribution) occurs, as shown by the left-going green arrow in Figure 5b. This charge redistribution tunneling (across a trapezoidal barrier) neutralizes charging such that the bond is again charge neutral, as indicated in Figure 5a. This completes the polar covalent bond formation tunneling cycle. As specified in Figure 5, polar covalent bonding involves asymmetric charge sharing facilitated by bidirectional tunneling across an asymmetric barrier. Bidirectional tunneling consists of cation-to-anion tunneling from and to neutral frontier orbitals (charge transfer) as well as anion-to-cation tunneling from and to charged frontier orbitals (charge redistribution). This type of bidirectional tunneling is characterized by unipolar charging in which the cation frontier orbital is neutral or positive, while the anion frontier orbital is neutral or negative.

Next, consider ionic bonding, as sketched in Figure 6, for the specific case of potassium bromide (KBr) in which it is

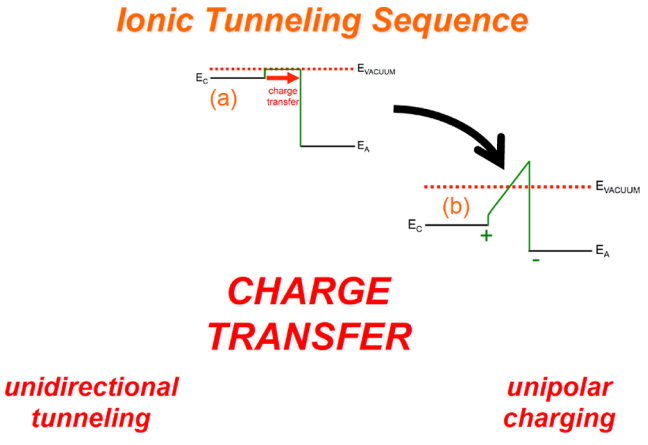


**Figure 6.** Heteropolar (ionic) bond formation tunneling sequence. (a) Electron tunnels from cation to anion frontier orbitals, leading to (b) negative (positive) charging of the anion (cation) frontier orbital. Tunneling then terminates. This figure illustrates bonding in potassium bromide (KBr) in which it is assumed that $E_C \approx -0.8$ eV, $E_A \approx -8.0$ eV, and $U_{\Delta q=1e^-} \approx 4.4$ eV.

assumed that $E_C \approx -0.8$ eV, $E_A \approx -8.0$ eV, and $U_{\Delta q=1e^-} \approx 4.4$ eV since $d \approx 330$ pm. As the cation and anion come toward one another from infinity, their frontier orbitals are energetically misaligned, as shown in Figure 6a. Comparing Figures 5a and 6a, it is evident that more frontier orbital misalignment occurs in ionic bonding than in polar covalent bonding. Nothing happens in terms of chemical bonding until the cation and anion are close enough that there is appreciable overlap


https://doi.org/10.1021/acsomega.3c02736
ACS Omega 2023, 8, 23182−23190

between their wave functions so that charge transfer occurs by quantum mechanical cation-to-anion tunneling of an electron across an asymmetric rectangular barrier, as shown by the right-going red arrow in Figure 6a. Electron tunneling leaves the cation positively charged, moving its frontier orbital downward in energy, while the anion is negatively charged, pushing the anion frontier orbital upward in energy, as given in Figure 6b. Additionally, a large electric field (130 MV/cm) is set up as a consequence of charge separation, as evident from the positive sloping portion of the barrier shown in Figure 6b.

After charge transfer, ionic bonding (Figure 6b) differs dramatically from that of covalent bonding (Figure 4b) since no heteropolar energetic driving force exists to move charge leftward, from the anion to the cation. Therefore, the ionic bonding sequence terminates abruptly after one electron "hops" from the cation to the anion. Thus, ionic bonding, as herein described, can be summarized as involving charge transfer via unidirectional tunneling and unipolar charging, as noted in Figure 6.

The attentive reader will recognize from an assessment of Figure 6b that a cation-to-anion energetic driving force still exists at the end of the ionic bonding sequence since the charged cation frontier orbital is positioned at a higher energy than that of the charged anion frontier orbital. For the case of KBr, as considered in Figure 6, only one electron occupies the K-cation frontier orbital. Thus, the ionic bonding sequence does indeed terminate for the KBr situation shown in Figure 6b. However, certain ionic compounds have two electrons occupying their cation frontier orbital. The ionic bond formation tunneling sequence differs for these materials, as discussed in the following.

If a second electron is indeed available in the cation frontier orbital, an alternative heteropolar bond tunneling sequence may apply, as pictured in Figure 7. Figure 7 is relevant to the specific case of bonding in barium oxide (BaO) in which it is assumed that $E_C \approx -2.2$ eV, $E_A \approx -6.6$ eV, and $U_{\Delta q=1e^-} \approx 5.2$ eV since d ≈ 276 pm. The first BaO charge transfer step, as shown in Figure 7a,b, is identical to that previously considered in Figure 6 for KBr. However, the right-going red arrow in Figure 7b indicates that a second electron tunnels (across a trapezoidal barrier) from the charged cation frontier orbital to the already charged anion orbital, rendering these orbitals doubly charged (Figure 7c).

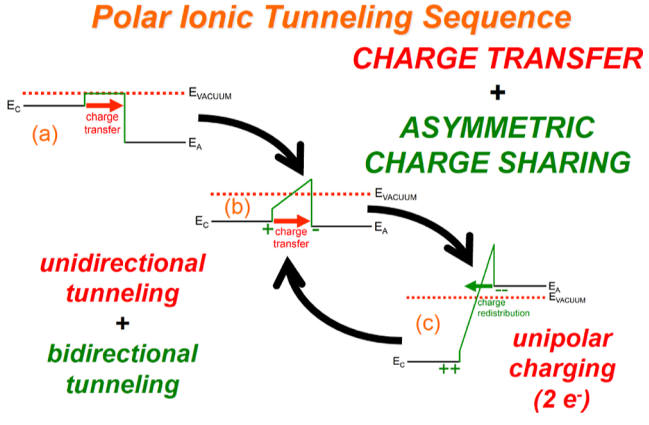


**Figure 7.** Heteropolar (polar ionic) bond formation tunneling sequence. (a) Electron tunnels from cation to anion frontier orbitals, leading to (b) negative (positive) charging of the anion (cation) frontier orbital. Next, a second electron tunnels from the cation to the anion, thereby (c) doubly charging the cation and anion frontier orbitals. Then, an electron tunnels from the anion to the cation, rendering the cation and anion frontier orbitals singly charged. This figure illustrates bonding in barium oxide (BaO) in which it is assumed that $E_C \approx -2.2$ eV, $E_A \approx -6.6$ eV, $U_{\Delta q=1e^-} \approx 5.2$ eV, and $U_{\Delta q=2e^-} = 4U_{\Delta q=1e^-} \approx 20.8$ eV.

Double charging means that the Coulombic energy due to charge separation is now exceedingly large, i.e., $U_{\Delta q=2e-} = 4U_{\Delta q=1e-} \approx 20.8$ eV. Additionally, the electric field dramatically increases to 760 MV/cm (Figure 7c) from 190 MV/cm (Figure 7b). Thus, there is a tremendously large driving force for electron tunneling from the anion to the cation (charge distribution, left-going green arrow in Figure 7c). This charge redistribution tunneling (Fowler-Nordheim tunneling across a triangular barrier of reduced thickness compared to $d_{BaO} = 276$ pm) resets the two-atom system back to the singly charged state of Figure 7b. Thus, polar ionic bonding is a two-electron process involving bidirectional tunneling in which charge transfer occurs by cation-to-anion tunneling from and to singly ionized frontier orbitals, while charge redistribution is accomplished by anion-to-cation tunneling from and to doubly ionized frontier orbitals. Also, an unusual type of unipolar charging occurs in which the cation frontier orbital is either singly or doubly positively charged, while the anion frontier orbital is either singly or doubly negatively charged.

**Chemical Bonding Summary.** Table 2 summarizes chemical bonding attributes as developed herein. Homopolar bonding (involving identical atoms) and covalent bonding are identical, whereas three types of heteropolar bonds (involving nonidentical atoms) are distinguished, i.e., polar covalent, ionic, and polar ionic. Covalent bonding is characterized by charge sharing via bidirectional tunneling across a symmetric barrier and bipolar charging in which each frontier orbital is alternately positively or negatively charged or neutral. In contrast, charge sharing is asymmetric for polar covalent and polar ionic bonding due to bidirectional tunneling across asymmetric barriers, while charge transfer via unipolar tunneling across an asymmetric barrier occurs in ionic bonding. All three types of heteropolar bonds involve asymmetric barriers and cation-to-anion charge transfer. Although chemists often assert certain types of heteropolar bonds to be "covalent", such bonds involving nonidentical atoms should more properly be designated "polar covalent," given the symmetry and charge state differences inherent between these two types of bonds, as revealed in Table 2.

**Table 2. Summary of Tunneling Aspects of Chemical Bonding**

| Bonding | Charge | Tunneling | Barrier |
|---|---|---|---|
| **Homopolar Bonding** | | | |
| covalent | sharing | | symmetric |
| **Heteropolar Bonding** | | | |
| polar covalent | transfer + redistribution | | asymmetric |
| ionic | transfer | | asymmetric |
| polar ionic | transfer + redistribution | | asymmetric |

**Simulated Tunneling Trends.** Chemical bonding tunneling trends are simulated using a point charge approximation to account for charge separation energy storage (via eq 3) and


https://doi.org/10.1021/acsomega.3c02736
ACS Omega 2023, 8, 23182−23190

assuming that energy barriers are both abrupt and piecewise-linear, as exemplified by the energy diagrams shown in Figures 4−7. Although these approximations are crude, their use in simulation reveals several interesting chemical trends.

First, we distinguish between forward and reverse tunneling. Forward tunneling involves an electron tunneling between two uncharged frontier orbitals. Reverse tunneling is the inverse process in which an electron present in the negatively charged frontier orbital tunnels to the positively charged frontier orbital, thereby resetting the system back into a charge-neutral state.

Figure 8a illustrates the case of heteropolar bonding in which forward tunneling is across an asymmetric rectangular barrier defined by two energy barrier parameters, $V_0$ and $V_1$, and the interatomic distance, $d$. In a heteropolar bond, forward tunneling is always from the cation to the anion since the anion frontier orbital is at a lower energy, i.e., $|E_C| < |E_A|$. For a specified $V_0$ and $V_1$, the forward tunneling transmission probability as a function of interatomic distance is equal to $T_F(d) = T_{0F} \exp(-d/d_F)$, where $T_{0F}$ is a forward tunneling pre-factor and $d_F$ is a forward tunneling characteristic distance.

The tunneling parameters $T_{0F}$ and $d_F$ are determined as follows. The tunneling transmission probability through an asymmetric rectangular barrier, $T(E)$, is estimated using[21]

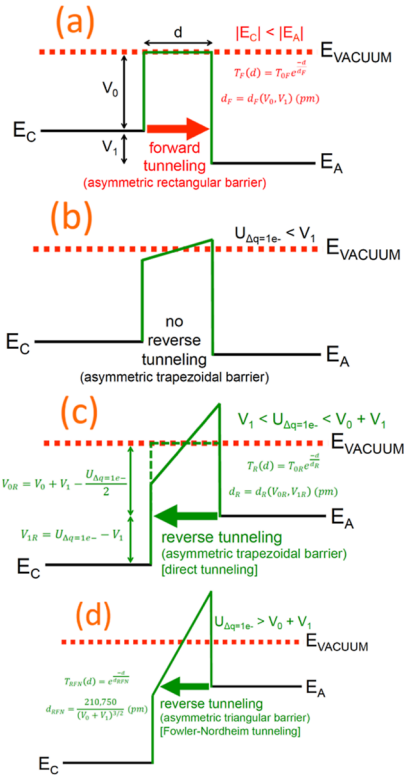


**Figure 8.** (a) Forward tunneling of an electron from a neutral cation frontier orbital to a neutral anion frontier orbital leads to a state in which the cation (anion) is positively (negatively) charged. (b) When $U_{\Delta q=1e^-} < V_1$, reverse tunneling is not possible since the charged anion frontier orbital is at a lower energy than the charged cation frontier orbital. (c) When $V_1 < U_{\Delta q=1e^-} < V_0 + V_1$, reverse tunneling occurs by direct tunneling across an asymmetrical trapezoidal barrier. (d) When $U_{\Delta q=1e-} > V_0 + V_1$, reverse tunneling occurs by Fowler−Nordheim tunneling across an asymmetric triangular barrier.

$$T(E) = \frac{\frac{4k_1k}{(k_1+k)^2}}{1 + \left[\frac{(k^2+\gamma^2)(k_1^2+\gamma^2)}{\gamma^2(k_1+k)^2}\right]\sinh^2(d\gamma)} \quad (4)$$

where

$$k_1 = \frac{\sqrt{2m(E+V_1)}}{\hbar}, \; k = \frac{\sqrt{2mE}}{\hbar}, \text{ and } \gamma = \frac{\sqrt{2m(V_0-E)}}{\hbar} \quad (5)$$

and where $m$ is the electron rest mass, $\hbar$ is the reduced Planck constant, $E$ is the tunneling energy (assumed in this analysis to be equal to the thermal energy at room temperature, i.e., 0.026 eV), $V_0$ is the forward tunneling barrier, and $V_0 + V_1$ is the reverse tunneling barrier ($V_0$, $V_1$ are positive quantities). For specified $V_0$ and $V_1$, $T_F(d)$ is simulated using eqs 4 and 5 for d's spaced every 20 pm between 100 and 400 pm. This $T_F(d)$ discrete data set is then curve fit via regression using the relationship $T_F(d) = T_{F0} \exp(-d/d_F)$. The quality of the regression fit is quite good, typically yielding a coefficient-of-determination, $R^2$, greater than 0.99.

Returning to Figure 8, notice that Figure 8b through 8d shows three possible reverse tunneling scenarios. When $U_{\Delta q=1e^-} < V_1$, as shown in Figure 8b, reverse tunneling is not possible since the charged anion frontier orbital is at a lower energy than that of the charged cation frontier orbital. This reverse tunneling situation corresponds to the case of ionic bonding in which tunneling is unidirectional. When $V_1 < U_{\Delta q=1e^-} < V_0 + V_1$, as shown in Figure 8c, reverse tunneling occurs by direct tunneling across an asymmetrical trapezoidal barrier. As shown in Figure 8c, reverse tunneling probability $T_R(d) = T_{R0} \exp(-d/d_R)$ is assessed via simulation and curve-fit regression using eqs 4 and 5 and tunneling parameters $V_{0R}$ and $V_{1R}$. These reverse tunneling parameters are obtained by recognizing that the original asymmetric trapezoidal barrier shown in Figure 8c can be replaced by an equivalent asymmetric rectangular barrier (dashed lines). Finally, Figure 8d applies when $U_{\Delta q=1e^-} > V_0 + V_1$, leading to an asymmetric triangular barrier such that reverse tunneling occurs by Fowler−Nordheim tunneling.

Table 3 summarizes tunneling parameters and tunneling equations used in the evaluation of ten semiconductors and insulators. The $d$, $V_0$, and $V_1$ entries in Table 3 are the only

**Table 3. Tunneling Parameters and Equations**[a]

| material | $d$ (pm) | $V_0$ (V) | $V_1$ (V) | $U_{\Delta q=1e^-}$ (eV) | $T_F$ | $T_R$ |
|---|---|---|---|---|---|---|
| C | 154 | 4.5 | 0 | 9.3 | $0.59\ e^{-d/45.45}$ | $e^{-d/22080}$ |
| Si | 235 | 4.5 | 0 | 6.1 | $0.59\ e^{-d/45.45}$ | $e^{-d/22080}$ |
| Ge | 245 | 4.5 | 0 | 5.9 | $0.59\ e^{-d/45.45}$ | $e^{-d/22080}$ |
| GaAs | 245 | 3.1 | 2.8 | 5.9 | $0.69\ e^{-d/55.56}$ | $e^{-d/14706}$ |
| GaN | 193 | 3.1 | 2.8 | 7.5 | $0.69\ e^{-d/55.56}$ | $e^{-d/14706}$ |
| MgTe | 293 | 2.2 | 4.4 | 4.9 | $0.65\ e^{-d/71.43}$ | $0.46\ e^{-d/47.62}$ |
| ZnO | 198 | 2.2 | 4.4 | 7.3 | $0.65\ e^{-d/71.43}$ | $0.69\ e^{-d/58.82}$ |
| BaO* | 276 | 2.2 | 4.4 | 5.2 | $0.36\ e^{-d/43.48}$ | $e^{-d/49720}$ |
| LiF | 201 | 0.8 | 7.2 | 7.2 | $0.40\ e^{-d/142.86}$ | 0 |
| KBr | 330 | 0.8 | 7.2 | 4.4 | $0.40\ e^{-d/142.86}$ | 0 |

[a] $d$ = interatomic distance; $V_0$ and $V_1$ = tunneling parameters (see Figure 8); $U_{\Delta q=1e^-}$ = Coulombic energy; and $T_F$ and $T_R$ = forward and reverse tunneling probabilities, respectively. * indicates that second-electron tunneling probabilities are used (see Figure 7).



https://doi.org/10.1021/acsomega.3c02736
ACS Omega 2023, 8, 23182−23190

three inputs required to accomplish a chemical bonding tunneling analysis. $U_{\Delta q=1e^-}$ is the Coulombic energy, as calculated using eq 3. $T_F$ and $T_R$ are the forward and reverse tunneling equations, respectively, in which prefactors and characteristic tunneling distances (units = pm) are explicitly indicated. Reverse tunneling occurs by Fowler−Nordheim tunneling for all of the Table 3 materials except for MgTe, ZnO, LiF, and KBr.

Table 4 captures highlights of tunneling trends obtained for a selected set of materials. $T_R/T_F$ is the ratio of reverse to forward tunneling transmission probability. When $T_R$ is large, reverse tunneling dominates so that occupancy of the uncharged state is favored. This can be quantified in an interesting way in terms of bond valence.[1] Bond valence, $s$, is equal to the amount of valence charge on an atom that gives rise to a specific bond. $s$ is measured in valence units (vu), where 1 vu is equal to the charge of an electron, i.e., $1.6 \times 10^{-19}$ C. According to one formulation of the bond valence model, the bond valence is described using Pauling's relationship $s = \exp[(d_0 - d)/b]$,[22] where $d_0$ is the interatomic distance of a single bond such that $s = 1$, $d$ is the actual interatomic distance, and $b$ is a constant. Rewriting Pauling's relationship as $s = s_0 \exp(-d/b)$, we recognize that this form is mathematically identical to that of our tunneling probability relationships, e.g., $T_F(d) = T_{0F} \exp(-d/b_F)$. Recognizing this and accounting for electron conservation lead to

**Table 4. Tunneling Trends**[a]

| Material | $T_F$ | $T_R$ | $T_R/T_F$ | s (vu) | PCT | Bonding Type |
|---|---|---|---|---|---|---|
| C | 0.0198 | 0.99 | 50 | 0.02 | NA | covalent |
| Si | 0.0033 | 0.99 | 300 | 0.003 | NA | covalent |
| Ge | 0.0027 | 0.99 | 367 | 0.003 | NA | covalent |
| GaAs | 0.0084 | 0.98 | 117 | 0.008 | 14.17 | strong polar covalent |
| GaN | 0.0214 | 0.99 | 46 | 0.02 | 9.32 | strong polar covalent |
| MgTe | 0.0107 | 0.0010 | 0.09 | 0.92 | 6.14 | weak polar covalent |
| ZnO | 0.0406 | 0.0239 | 0.59 | 0.63 | 4.6 | weak polar covalent |
| BaO | 0.0006* | 1.0* | 1667* | 1.0006 | 2.06 | ionic |
| LiF | 0.3664 | 0 | 0 | 1.0 | 1.75 | ionic |
| KBr | 0.0398 | 0 | 0 | 1.0 | 1.42 | ionic |

[a] $T_F$ and $T_R$ = forward and reverse tunneling probabilities; s = bond valence; and PCT = polar covalent tendency. *Color code*: black = covalent; blue = strong polar covalent (PCT > 7); red = weak polar covalent (PCT = 3−7); and green = ionic (PCT = 0−3). * indicates that these are second-electron tunneling probabilities (see Figure 7).

$$s = \frac{1}{1 + \frac{T_R}{T_F}} \tag{6}$$

Equation 6 simply states that the bond valence is established by the probability of tunneling out of a charged frontier orbital ($T_R$) compared to the probability of tunneling out of a neutral frontier orbital ($T_F$). This formulation of bond valence asserts that tunneling is the physical process underlying the bond valence model.

Now focus on the last three columns of Table 4. There is a strong correlation between the bond valence and PCT. Covalent and strongly polar covalent bonding involves almost no bond valence charge. Although electron tunneling is very intense and occurs on extraordinarily short time scales (see Table 1) for these covalent and strongly polar covalent materials, very little charge is actually present in a time-averaged sense in the charged frontier orbital state since reverse tunneling overwhelmingly dominates. This observation makes it hard to see why the covalent interaction is so strong, unless covalent tunneling is essentially a resonance phenomenon, as previously proposed.[1] In contrast, weak polar covalent bonding involves a significant amount of bond valence charge. Although electrons tunnel in both directions in the case of weak polar covalent bonding, they spend significantly more time in the charged state of the anion frontier orbital than in the uncharged state of the cation frontier orbital.

Finally, the bond valence is equal to one for the case of normal ionic bonding. Tunneling is unidirectional. After an electron undergoes forward tunneling from the cation to the anion, it is trapped in the charged anion frontier orbital because it is at a lower energy than the charged cation frontier orbital. In the unusual situation of two-electron tunneling, as is for the case of polar ionic bonding for BaO (Figure 7), the first-to-tunnel electron contributes all of its charge to the bond valence, while the second-to-tunnel electron contributes almost none of its charge to the bond valence. Given the gigantic reverse electric field set up after second-electron tunneling (see Figure 7c), this is not surprising; the second-to-tunnel electron is essentially ripped out of the doubly charged anion frontier orbital by extremely intense Fowler−Nordheim reverse tunneling.

Two additional take-aways are obtainable from an assessment of Table 4. First, a comparison of Table 4 and Figure 8 reveals that the nature of reverse tunneling determines whether a heteropolar bond is ionic, weakly polar covalent, or strongly polar covalent. When reverse tunneling does not occur (Figure 8b), the heteropolar bond is ionic. When reverse tunneling occurs by direct tunneling (Figure 8c), the heteropolar bond is weakly polar covalent. When reverse tunneling occurs by Fowler−Nordheim tunneling (Figure 8d), the heteropolar bond is strongly polar covalent. Second, as defined by eq 6, the bond valence, $s$, pertains to the forward tunneling final state atom, i.e., the anion in the case of a heteropolar bond. This means that the forward tunneling initial state atom, i.e., the cation in the case of a heteropolar bond, has a bond valence equal to $1 - s$.

A comparison of Tables 3 and 4 indicates that tunneling parameter $V_0$ to a large extent determines $T_F$. Thus, the cation frontier orbital energy is dominant in establishing the forward tunneling probability. In contrast, the situation is more complicated for the reverse tunneling case, as $T_R$ depends primarily not only on $V_1$ and $d$ (which determines $U_{\Delta q=1e^-}$) but also (to a lesser extent) on $V_0$. The fact that the $T_R$ tendency with respect to tunneling parameters is more complicated than that of $T_F$ is consistent with the picture provided in Figure 8 in which the forward tunneling process is unique, whereas three different paths exist to accomplish reverse tunneling.

Determining frontier orbital energies is a key challenge for accomplishing a chemical bonding tunneling analysis. We rely on atomic SSE trends to estimate frontier orbital energies. Average atomic SSEs (⟨SSE⟩) as a function of oxidation state are indicated in Table 5, where ⟨SSE⟩ is measured with respect


https://doi.org/10.1021/acsomega.3c02736
ACS Omega 2023, 8, 23182−23190

Table 5. Oxidation State, Formal Charge, and Average Atomic Solid-State Energy[13]

| oxidation state | formal charge | ⟨SSE⟩ (eV) |
|---|---|---|
| +1 | -3 | -0.8 |
| +2 | -2 | -2.2 |
| +3 | -1 | -3.1 |
| +4 | 0 | -3.4 |
| +5 | 0 | -3.8 |
| +6 | 0 | -4.6 |
| -3 | +1 | -5.9 |
| -2 | +2 | -6.6 |
| -1 | +3 | -8.0 |

to the vacuum level.[13] Although a clear trend is evident, it is hard to quantify this trend using the oxidation state as an independent variable. However, this problem is circumvented if the charge state is specified in terms of formal charge. Then, the trend can be discerned by plotting ⟨SSE⟩ as a function of formal charge, as accomplished in Figure 9.

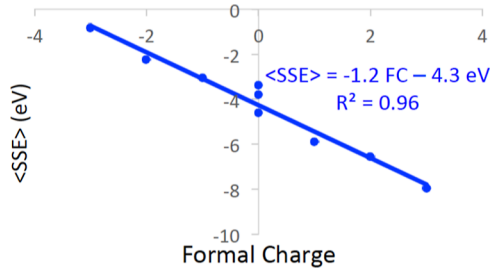


Figure 9. Average atomic SSE (⟨SSE⟩) versus formal charge.

The trend shown in Figure 9 is quite remarkable. According to the SSE database, ⟨SSE⟩ depends linearly on the formal charge. We have used values of ⟨SSE⟩ listed in Table 5 as frontier orbital estimates for accomplishing chemical bonding tunneling analysis. For example, Table 3 shows that $V_0$ = 3.1 V and $V_1$ = 2.8 V for both GaAs and GaN. $V_0$ corresponds to the +3 oxidation state (or −1 formal charge) entry of Table 5, except for a difference in sign since energy and potential (voltage) have opposite signs. Also, the sum $V_0 + V_1$ is equal to 5.9 V, corresponding (except for the sign) to the −3 oxidation state (or +1 formal charge) entry of Table 5. Note that for the elements C, Si, and Ge, we assume a frontier orbital energy of −4.5 eV, corresponding to the hydrogen donor/acceptor ionization energy, $\varepsilon(\pm)$.

**Tunnel Barrier Actual Shape.** When two identical or dissimilar atoms are positioned far from one another such that their wave function overlap is negligible, as shown in Figures 4a and 5a, respectively, the resulting tunneling barriers are likely to be abrupt and piecewise linear, as indicated in these figures. However, when these atoms are in close physical proximity such that chemical bonding occurs, the tunnel barrier shapes shown in Figures 4−7 are idealized since the tunnel barrier shapes shown are obtained assuming a point charge model for the two atoms forming molecular orbitals.

A more realistic picture of what the tunnel barrier might look like is given in Figure 10 for the cases of covalent and polar covalent bonding. Note that these more realistic barriers are neither abrupt nor piecewise linear. The shapes of these barriers are sketched in accordance with energy band diagram considerations.[23] The negative curvature shown for the

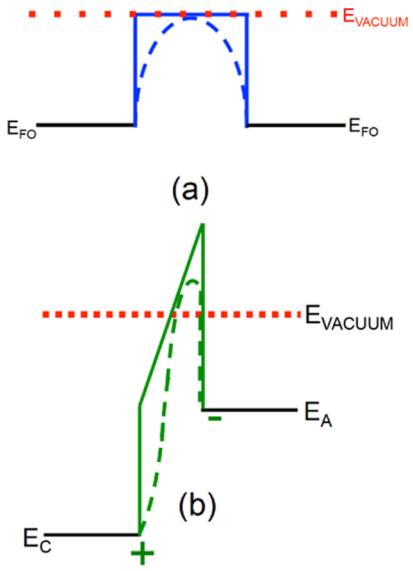


Figure 10. Idealized (solid lines) and more realistic (dashed lines) tunnel barrier shapes for the case of (a) covalent bonding and (b) polar covalent bonding.

covalent barrier in Figure 10a indicates the presence of the negative charge within the barrier. In contrast, the positive curvature indicated on the left side of Figure 10b reveals the existence of the positive charge near the cation, while the negative curvature shown on the right side of Figure 10b shows that the negative charge is present near the anion.

The most important aspect of Figure 10 is the notable symmetry of the tunnel barrier for covalent bonding and the pronounced asymmetry of the tunnel barrier for polar covalent bonding. All aspects of homopolar and heteropolar bond formation are dominated by the symmetric or asymmetric nature, respectively, of the tunnel barrier.

As a final note, although we have modeled the tunneling transmission probability as $T(d) = T_0 \exp(-d/b)$, physical considerations suggest that $T(d) = \exp(d/b)$, in which the tunneling transmission prefactor is suppressed, i.e., is set equal to one, may be a more appropriate formulation. This is because the tunneling transmission prefactor arising from the use of eqs 4 and 5 accounts for quantum mechanical reflection of a propagating electron encountering an abrupt energy barrier.[18] However, quantum mechanical reflection is not expected to be relevant for the tunneling case under consideration involving an electron tunneling between two atomically constrained states. Regardless of whether the tunneling prefactor is included or suppressed in the assessment of the tunneling transmission probability, quantitative bonding trends such as those shown in Table 4 are little impacted. For example, ignoring the tunneling prefactor changes the bond valence of Si from 0.003 to 0.006 vu, of GaAs from 0.008 to 0.012 vu, and of MgTe from 0.92 to 0.89 vu.

## CONCLUSIONS

Chemical bonding and quantum mechanical electron tunneling are intimately linked. Covalent bonding involves bidirectional tunneling across a symmetric energy barrier and bipolar charging of frontier orbitals. Polar covalent and polar ionic bonding rely on bidirectional tunneling across asymmetric energy barriers and unipolar charging. In contrast, ionic bonding occurs via unidirectional tunneling from the cation to


https://doi.org/10.1021/acsomega.3c02736
ACS Omega 2023, 8, 23182−23190

the anion across an asymmetric energy barrier and unipolar charging. We propose that electron tunneling is the physical mechanism underlying the widespread application of the bond valence method in chemistry, physics, and materials science.

The *dynamic* (time-*dependent* Schroedinger equation) perspective employed herein sometimes provides more insights than the conventional *static* (time-*independent* Schroedinger equation) perspective upon which most of the chemistry is based. For example, according to molecular orbital theory, it is the exchange integral that stabilizes the chemical bond. However, what does this mean? What is the physics underlying this stabilization? The *static* perspective provides no physical insights here, except that chemical stabilization is quantum mechanical in nature and that it is perhaps a bit mysterious. In contrast, by adopting the d*ynamic* perspective advocated herein, these issues are simply and easily clarified, i.e., chemical bond stabilization is coulombic in nature and occurs as a consequence of charge separation arising from forward and reverse tunneling.

## AUTHOR INFORMATION


### Corresponding Author

**Douglas A. Keszler** − *Department of Chemistry, Oregon State University, Corvallis, Oregon 97331-4003, United States;* orcid.org/0000-0002-7112-1171; Email: Douglas.Keszler@oregonstate.edu

### Author

**John F. Wager** − *School of EECS, Oregon State University, Corvallis, Oregon 97331-5501, United States;* orcid.org/0000-0002-8992-1847

Complete contact information is available at: https://pubs.acs.org/10.1021/acsomega.3c02736


### Notes

The authors declare no competing financial interest.

## ACKNOWLEDGMENTS

This material is based upon work supported by the National Science Foundation under grant no. CHE-1606982.

## ABBREVIATIONS

EA, electron affinity; IP, ionization potential; SSE, solid-state energy; PCT, polar covalent tendency

## REFERENCES


(1) Brown, I. D. *The Chemical Bond in Inorganic Chemistry*; Oxford University Press, 2016.

(2) Libby, W. F. Electron tunneling in chemistry and biology. *Annu. Rev. Phys. Chem.* **1977**, *28*, 105−110.

(3) Bell, R. P. *The Tunnel Effect in Chemistry*; Springer, 1980.

(4) Gol'danskii, V. I.; Trakhtenberg, L. I.; Fleurov, V. N. *Tunnel Phenomena in Chemical Physics*; Gordon and Breach, 1989.

(5) Khairutdinov, R. F.; Zamaraev, K. I.; Zhadanov, V. P. *Electron Tunneling in Chemistry*; Elsevier, 1989.

(6) McMahon, R. J. Chemical reactions involving quantum tunneling. *Science* **2003**, *299*, 833−834.

(7) Nakumura, H.; Mil'nikov, G. *Quantum Mechanical Tunneling in Chemical Physics*; CRC Press, 2013.

(8) Schreiner, P. R. Quantum Mechanical Tunneling Is Essential to Understanding Chemical Reactivity. *Trends Chem.* **2020**, *2*, 980−989.

(9) Putz, M. V. Chemical bonding as quantum tunneling: the Capra bondons. *Fullerenes, Nanotubes Carbon Nanostruct.* **2022**, *30*, 979−986.

(10) Sutton, A. P. *Electronic Structure of Materials*; Clarendon Press, 1993.

(11) Huheey, J. E.; Keiter, E. A.; Keiter, R. L. *Inorganic Chemistry: Principles of Structure and Reactivity*, 4th ed.; HarperCollins, 1993; p. 156-157.

(12) Pelatt, B. D.; Ravichandran, R.; Wager, J. F.; Keszler, D. A. Atomic Solid State Energy Scale. *J. Am. Chem. Soc.* **2011**, *133*, 16852−16860.

(13) Pelatt, B. D.; Kokenyesi, R. S.; Ravichandran, R.; Pereira, C. B.; Wager, J. F.; Keszler, D. A. Atomic solid state energy scale: Universality and periodic trends in oxidation state. *J. Solid State Chem.* **2015**, *231*, 138−144.

(14) Ravichandran, R.; Wang, A. X.; Wager, J. F. Solid state dielectronic screening versus band gap trends and implications. *Opt. Mater.* **2016**, *60*, 181−187.

(15) Pelatt, B. D.; Wager, J. F.; Keszler, D. A. Elucidation of bonding trends from variability in Atomic Solid State Energies. *J. Solid State Chem.* **2019**, *274*, 337−351.

(16) Penn, D. R. Wave-Number-Dependent Dielectric Function of Semiconductors. *Phys. Rev.* **1962**, *128*, 2093−2097.

(17) Phillips, J. C.; Lucovsky, G. *Bonds and Bands in Semiconductors*, 2nd ed.; Momentum Press, 2009.

(18) Eisberg, R. M. *Fundamentals of Modern Physics*; Wiley, 1961.

(19) Cheng, D. K. *Field and Wave Electromagnetics*; Addison-Wesley, 1983; p 71.

(20) Sze, S. M.; Ng, K. K. *Physics of Semiconductor Devices*, 3rd ed.; Wiley, 2007.

(21) Ferry, D. K.; Goodnick, S. M.; Bird, J. *Transport in Nanostructures*; Cambridge University Press, 2009.

(22) Pauling, L. Atomic Radii and Interatomic Distances in Metals. *J. Am. Chem. Soc.* **1947**, *69*, 542−553.

(23) Wager, J. F.; Kuhn, K. Device Physics Modeling of Surfaces and Interfaces from an Induced Gap State Perspective. *Crit. Rev. Solid State Mater. Sci.* **2017**, *42*, 373−415.




https://doi.org/10.1021/acsomega.3c02736
*ACS Omega* 2023, 8, 23182−23190